Chinese Physics Letters

LETTER

Thermal and Electrical Conductivities of Aluminum Up to 1000 eV: A First-Principles Prediction

Cite as: Qianrui Liu *et al*. 2026 *Chin. Phys. Lett.* **43** 070501

DOI CSTR

Recommended Articles

First-Principles Study on Thermal and Electrical Transport Properties of $NbGe_2$ and $NbSi_2$: The Role of Electron–Phonon Coupling
Gui-Lin Zhu, Man-Yu Shang, and Jing-Tao Lü
Chin. Phys. Lett. **41**, 126301 (2024)

Data-Driven Prediction of Thermal Conductivity from Short MD Trajectories: A GCN-LSTM Approach
Shihao Feng, Haifeng Chen, Jian Zhang, Meng An, and Gang Zhang
Chin. Phys. Lett. **43**, 020801 (2026)

Four-Phonon Scattering and Wave-Like Phonon Tunneling Drive Glassy Ultralow Lattice Thermal Conductivity in $Cs_2AgInCl_6$
Rongrong Ma, Xiaoxiao Zhang, Shiqi Guo, Mei Ge, Junfeng Zhang, and Jiangjiang Ma
Chin. Phys. Lett. **42**, 090709 (2025)

Experimental Investigation of the Anisotropic Thermal Conductivity of C/SiC Composite Thin Slab
Ke-Fan Wu, Hu Zhang, and Gui-Hua Tang
Chin. Phys. Lett. **41**, (2024)

Thermal and Electrical Percolation Transport Behavior in Composite Materials with Oriented Binary Fillers
Jinxin Zhong, Zhuoyu Wang, Xiaokun Gu, Jun Wang, Yuanyuan Wang, and Xin Qian
Chin. Phys. Lett. **42**, 080602 (2025)

Theoretical Models on Interfacial Thermal Conductance of Nanoscale Solid Interfaces in Chips: A Mini Review
Zhicheng Zong *et al*.
Chin. Phys. Lett. **41**, 106301 (2024)

A series journal of Chinese Physical Society distributed by IOP Publishing

Chinese Physics Letters

Chin. Phys. Lett. **43** 070501 (2026)

LETTER

DOI: 10.1088/0256-307X/43/7/070501
CSTR: 32039.14.0256-307X.43.7.070501

Thermal and Electrical Conductivities of Aluminum Up to 1000 eV: A First-Principles Prediction

Qianrui Liu(刘千锐)[1], Xiantu He(贺贤土)[1,2], and Mohan Chen(陈默涵)[1,*]

[1]HEDPS, CAPT, School of Mechanics and Engineering Science and School of Physics, Peking University, Beijing 100871, China
[2]Institute of Applied Physics and Computational Mathematics, Beijing 100088, China

[*]Corresponding author. Email: mohanchen@pku.edu.cn

Accurate prediction of the thermal and electrical conductivities of materials under extremely high temperatures is essential in high-energy-density physics. These properties govern processes such as stellar core dynamics, planetary magnetic field generation, and laser-driven plasma evolution. However, first-principles methods like Kohn-Sham (KS) density functional theory (DFT) face challenges in predicting these properties due to prohibitively high computational costs. We propose a scheme that integrates the Kubo formalism with a mixed stochastic-deterministic DFT (mDFT) method, which substantially enhances efficiency in computing thermal and electrical conductivities of dense plasmas under extremely high temperatures. As a showcase, this approach enables *ab initio* calculations of the thermal and electrical conductivities of aluminum (Al) up to 1000 eV. Compared to traditional transport models, our first-principles results reveal significant deviations in the thermal and electrical conductivities of Al within the warm dense matter regime, underscoring the importance of accounting for quantum effects when investigating these transport properties of warm dense matter.

Introduction

Accurate prediction of thermal and electrical conductivities in dense plasmas is crucial for advancing research in astrophysics and inertial confinement fusion (ICF). Thermal conductivity is critical for studying the structures and evolution of planetary cores [1−3]. Additionally, it plays a significant role in the development of ablator materials and internal fuel capsules [4−6], as well as in the interactions between laser and targets [7], which are important for designing ICF experiments. Electrical conductivity, on the other hand, plays a key role in understanding the metallization of high-pressure hydrogen [8−10] and helium [10−13], which is essential for modeling the interiors of gas giants and brown dwarfs.

Measuring thermal conductivity experimentally remains challenging [14−16]. For instance, determining the thermal conductivity of dense plasmas is severely constrained by their extreme conditions and short lifetimes. While the Wiedemann-Franz law enables direct estimation of thermal conductivity from electrical conductivity in certain low-temperature experiments [17,18], this relationship breaks down for dense plasmas due to the temperature dependence of the Lorenz number [14], which is defined as the ratio of thermal to electrical conductivities scaled by temperature. Furthermore, despite the existence of various simulation models designed to describe thermal and electrical conductivities of dense plasmas, such as Spitzer [19,20], Lee−More [21], and Ichimaru [22], the accuracy of these models is still limited. The first-principles approach based on Kohn−Sham Density Functional Theory (KSDFT) [23−25] and the Kubo−Greenwood formula [26,27] has been widely used for predicting the conductivities of materials [28−32]. However, KSDFT faces significant challenges at high temperatures due to the rapid, cubic ($O(T^3)$) increase in computational cost with temperature [33]. In this regard, quantum Monte Carlo (QMC) was proposed as an alternative first-principles method for calculating the electrical conductivity around a decade ago [34]. Moreover, although methods based on the average-atom (AA) model have been proposed to cover a broader temperature range for dense plasmas [35−38], their accuracy requires rigorous validation against first-principles results.

The mixed stochastic-deterministic density functional theory (mDFT) [39] is a promising alternative to conventional KSDFT for high-temperature systems. It combines the precision of KSDFT with the high-temperature efficiency of stochastic density functional theory (sDFT) [33,40], achieved by using stochastic wave functions rather than explicitly diagonalizing the Hamiltonian. Unlike pure sDFT, the mDFT approach explicitly treats low-energy, tightly bound states with deterministic Kohn–Sham orbitals. This improves accuracy while remaining computationally inexpensive and simultaneously reduces stochastic noise. While sDFT-based methods for electrical conductivity have been developed [41], their application to dense plasmas has remained limited, primarily due to non-negligible stochastic noise. Moreover, to the best of our knowledge, no efficient first-principles methods for calculating thermal conductivity at extremely high temperatures have been reported to date, despite it being more challenging to measure experimentally.

We present a unified first-principles methodology within the mDFT framework for computing both electrical and thermal conductivities from Onsager coefficients across a wide temperature range, including the hot dense plasma regime. Our method yields results in close agreement with those obtained using the Kubo-Greenwood approach of KSDFT, while offering greater efficiency for high-temperature systems. More details can be found in the Supplementary Materials (SM). We apply this approach to calculate the electrical and thermal conductivities of aluminum (Al) over a broad temperature range, extending first-principles calculations from the few-tens-of-eV limit of conventional KSDFT to 1000 eV, where electrons are nearly fully ionized.

Methods

Both sDFT and mDFT methods do not directly yield all occupied eigenvalues, and instead, they compute physical properties based on the trace of the corresponding quantum mechanical operators. In this context, conductivities can be derived from the current response function, as described by the Kubo formula [26], where the response function is expressed in terms of the trace of the current operator

Received 23 March 2026; accepted 25 May 2026; published 22 July 2026

© 2026 Chinese Physical Society and IOP Publishing Ltd. All rights, including for text and data mining, AI training, and similar technologies, are reserved.

Check for updates

$$C_{nm}(t) = -\frac{i}{\hbar}\theta(t)\mathrm{Tr}\left\{\hat{f}_{\mathrm{H}}\left[\hat{\boldsymbol{j}}_n, \hat{\boldsymbol{j}}_m(t)\right]\right\}, \quad (1)$$

where $[,]$ denotes the commutator, $\theta(t)$ is the Heaviside step function, and $\hat{f}_{\mathrm{H}}$ is the Fermi−Dirac function of the Hamiltonian operator $\hat{H}$, which represents the density matrix $\hat{\rho}$ in the single-particle system. The operator $\hat{\boldsymbol{j}}_1$ and $\hat{\boldsymbol{j}}_2$ represent the electrical and heat current, respectively. In the present work, the two current operators are taken along the same direction, corresponding to longitudinal transport. Transverse conductivities can be obtained by choosing different directions.

To calculate conductivities, we employ mixed KS-stochastic orbitals to evaluate the trace in the current response function shown in Eq. (1), rather than relying solely on stochastic orbitals. This hybrid strategy reduces stochastic errors and improves efficiency, particularly when treating tightly bound core states. In addition, representing low-energy core electrons with KS orbitals raises the minimum energy in the stochastic subspace, thereby narrowing the spectral width and substantially decreasing the order required in the Chebyshev expansion used for time propagation, which further enhances computational efficiency. Since existing stochastic DFT formulations [41] are not directly applicable to mixed KS-stochastic orbitals, we derived a new trace expression (see the SM for details), given by

$$T_{nm}(t) = \sum_{a,b}\left\langle\varphi_a^{+}\left(\frac{t}{2}\right)\middle|\hat{\boldsymbol{j}}_n\middle|\varphi_b^{-}\left(\frac{t}{2}\right)\right\rangle\times\left\langle\varphi_b^{-}\left(-\frac{t}{2}\right)\middle|\hat{\boldsymbol{j}}_m\middle|\varphi_a^{+}\left(-\frac{t}{2}\right)\right\rangle, \quad (2)$$

where T_{nm} is the trace part in Eq. (1) and the time-evolved states are defined by

$$\left|\varphi^{+}\left(\frac{t}{2}\right)\right\rangle \equiv \exp(\mathrm{i}\hat{h}t/2)\hat{f}_{\mathrm{H}}^{1/2}\left|\varphi\right\rangle,$$
$$\left|\varphi^{-}\left(\frac{t}{2}\right)\right\rangle \equiv \exp(\mathrm{i}\hat{h}t/2)(1-\hat{f}_{\mathrm{H}})^{1/2}\left|\varphi\right\rangle, \quad (3)$$

with $\hat{h} = \hat{H}/\hbar$ and $|\varphi\rangle$ denoting KS or stochastic orbitals. For KS orbitals, the above expressions reduce to simple substitutions of their eigen energies, avoiding any additional computation.

We performed molecular dynamics (MD) simulations of aluminum at a density of 2.7 g/cm^3 and a temperature range of 10–1000 eV with the ABACUS package [42−44]. Simulation cells contained 32 atoms for temperatures up to 30 eV, 16 atoms for temperatures up to 200 eV, and 4 atoms for higher temperatures. Each simulation was run for 2000 steps with a time step of $r_s/60\bar{v}$, where r_s is the Wigner−Seitz radius and $\bar{v}$ is the average velocity. The temperature was controlled by the Nosé−Hoover thermostat [45,46], which is widely employed in first-principles molecular dynamics simulations of dense plasmas [30−32,47]. Since the temperature-dependent exchange-correlation (XC) functionals such as KSDT [48,49] have only a minor impact on the results [50], we adopted the Perdew-Burke-Ernzerhof (PBE) exchange-correlation functional [51], with a $2\times2\times2$ Brillouin zone sampled using the Monkhorst−Pack method [52]. We then selected 5 configurations, which are sufficient to ensure that the relative error of mDFT is below 10% to calculate the current response functions using the approach outlined in Eq. (1). Here, only the electronic contribution to conductivity is considered, as the ionic part is negligible [32]. To ensure accuracy, we used pseudopotentials with 13 valence electrons for calculating conductivities at $T > 10$ eV, while at 10 eV results with 11 and 13 valence electrons agree well. It is worth noting that, due to computational limitations, we did not directly test system-size convergence for the 13-electron pseudopotential at high temperatures. Instead, tests performed for the 11-electron case show well-converged results, suggesting that size effects in the 13-electron calculations are expected to be small. To illustrate the efficiency of the present approach, we estimate KSDFT scaling as $O(T^3)$ using our computational setup (dual-socket Intel Xeon Platinum 8462Y+, 128 cores). Over 500–1000 eV, KSDFT requires months to a year of wall time and ~0.5–2 TB of memory, whereas mDFT completes in ~3–8 days with tens of GB memory.

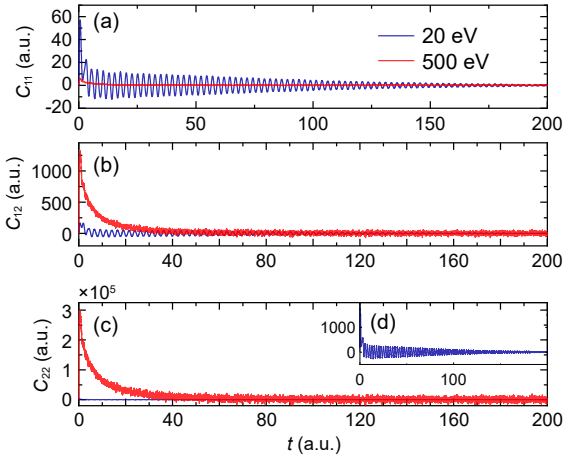

Fig. 1. Current response functions C_{mn} of aluminum, at $T = 20$ eV (blue) and $T = 500$ eV (red), including (a) C_{11}, (b) C_{12}, and (c) and (d) C_{22}. Panel (d) shows the same data as in (c) but with the vertical scale enlarged by 100× for clarity.

Results and Discussion

Figure 1 shows the current response functions C_{mn} of aluminum at $T = 20$ and 500 eV. C_{mn} curves exhibit oscillatory structures, with notable differences attributed to different energy levels. At low temperature (20 eV), electron transitions occur within a narrow energy range, resulting in well-defined, sharp oscillations in the frequency domain. At high temperature (500 eV), the introduction of higher-energy states leads to broadband excitation, causing the oscillations to be more complex and irregular due to the superposition of many transitions. Furthermore, for the response of electrical current C_{11}, the calculation at 20 eV produces higher magnitudes. However, for that of heat current C_{22}, the inclusion of higher energy levels at 500 eV results in higher magnitudes. Additionally, the response function decays more rapidly towards zero at lower temperatures, implying a smaller relaxation time.

Figure 2 illustrates the *ab initio* electrical and thermal conductivities of Al up to 1000 eV. Results from mDFT (red solid stars) and KSDFT (dark red hollow circles) are in close agreement, establishing the accuracy of mDFT for transport calculations. The electrical conductivity decreases with temperature before rising again, with a minimum near 20 eV, which is associated with the onset of L-shell ionization and the thermal excitation of electrons to higher-energy states, as discussed later. In contrast, the thermal conductivity increases monotonically, with a change in slope around 20 eV.

A comparison with existing models shows a marked discrepancy in their agreement. The effective ion charges used in the Lee−More model in this comparison are obtained from KSDFT and mDFT calculations, while the Spitzer model employs the full set of ion charges. Although the Lee−More model [21] captures the characteristic minimum in electrical conductivity, its accuracy at lower temperatures differs markedly from our first-principles results, and the position of this minimum also varies. When temperatures are above 200 eV, its results agree well with mDFT results. Conversely, since the Spitzer model [19] assumes full ionization, its results deviate from ours at lower temperatures but begin to converge as the temperature increases. Average-atom (AA) models often incorporate adjustable parameters and model-dependent choices, leading to varied outcomes. For instance, Shaffer and Starrett's model [36], which integrates the quantum Landau-Fokker-Planck equation and mean-force scattering, generally reproduces the first-principles results well, despite some minor differences in detail. In contrast, Wetta and Pain's model [37], which combines the Ziman formalism, yields results that are notably lower than Shaffer and Starrett's at high temperatures. This underscores that different average-atom models, due to their inherent adjustable parameters, can produce inconsistent and sometimes significantly divergent outcomes. In comparison with the Spitzer and Lee–More

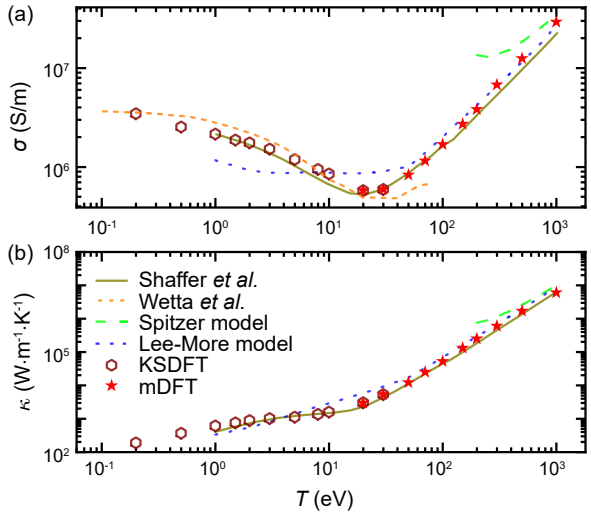

Fig. 2. (a) Electrical conductivity σ and (b) thermal conductivity κ of Al from 0.2 to 1000 eV. Shown for comparison are traditional plasma transport models, including the Spitzer model [19] (green line) and the Lee–More model [21] (blue line). Results based on average-atom models are also plotted: Shaffer and Starrett [36] (yellow-gray line) and Wetta and Pain [37] (orange line). First-principles calculations are given by KSDFT (dark red open hexagon) and mDFT (red stars). For $T < 10$ eV, KSDFT results are taken from our previous work [50].

formulations, our approach more consistently accounts for quantum effects, while, relative to AA models, it explicitly incorporates ionic structure effects. Therefore, our parameter-free first-principles calculations are crucial. They provide invaluable, robust reference data, establishing a new standard for validating and refining future modeling efforts in this field.

Figure 3 illustrates the capability of the present method to calculate high-temperature properties. Stochastic orbitals are effective in capturing the electronic information of high-energy levels. At low temperatures, the contribution from high-energy states is negligible [as shown in Fig. 3(a)], allowing a limited set of KS orbitals to provide converged results. However, as the temperature increases, the contribution from high-energy states becomes more significant. For example, at 100 eV, the contributions from the finite KS orbitals and the high-energy states are comparable. As the temperature rises to 1000 eV, the contribution from the finite KS orbitals becomes almost negligible, making stochastic orbitals crucial. This highlights the inefficiency of relying solely on KS orbitals at such extreme temperatures. Despite having only 96 stochastic orbitals, figure 3(c) shows that the orthogonalized stochastic orbitals provide a statistical representation of the high-energy states, with the stochastic error controlled by the number of orbitals. As shown in the SM, these errors are small, resulting in accurate conductivities.

Using the Drude model, the relationship for thermal conductivity is given by

$$\kappa = \frac{\tau}{3} C_V \bar{v}^2, \tag{4}$$

which leads to the concept of specific heat at constant volume (C_V). Here τ is the relaxation time. In the regime where $T \ll T_F$ (strong degeneracy), the specific heat is proportional to the temperature, and therefore Lorenz number remains constant, which is $(\pi^2/3)(k_B/e)^2$. However, as the temperature approaches T_F, higher-order temperature terms start to appear in the specific heat, causing it to decrease. This results in a reduction of $\kappa/\sigma T$, a phenomenon widely observed in previous computational studies. For temperatures much greater than T_F (weak degeneracy), the specific heat follows the classical result of the equipartition theorem, $(3/2)\cdot 13$, and aluminum, as a dense metallic system, adheres to this result at both high and low temperatures.

Figure 4(b) shows the effective ion charge at varying temperatures, defined as the number of electrons occupying the continuum

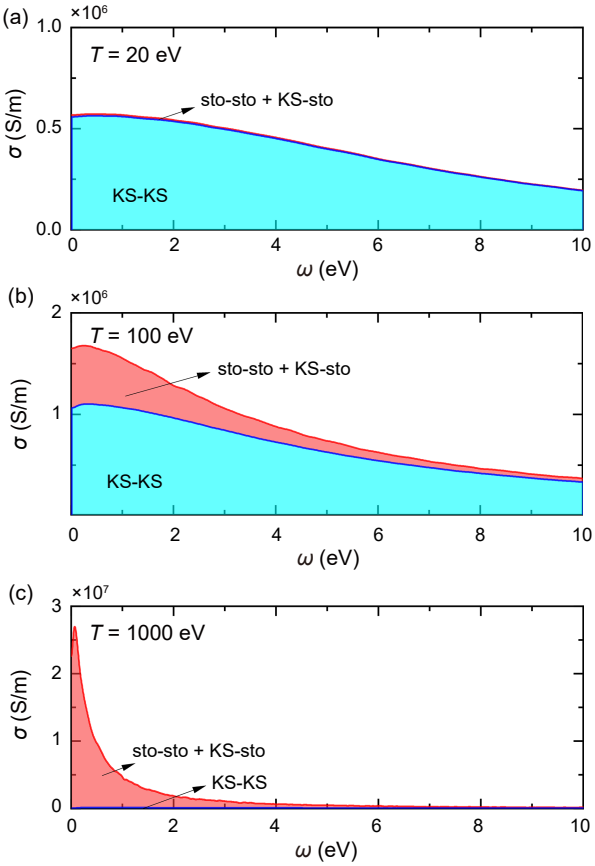

Fig. 3. Contributions to electrical conductivities of different orbitals at temperatures of (a) 20 eV, (b) 100 eV, and (c) 1000 eV. Blue regions represent the contributions from pure KS orbitals (KS-KS). Red regions denote the additional contributions from mixed stochastic orbitals, which include both transitions between KS and stochastic orbitals (KS-sto) and transitions among stochastic orbitals themselves (sto-sto). It is worth noting that, for DC electrical and thermal conductivities, the sto–sto component dominates the contributions from mixed stochastic orbitals.

(unbound) states per atom. It indicates that the first noticeable rise in the effective ion charge Z^* occurs near $T \approx 10$ eV, corresponding to the ionization of the L-shell electrons. This process increases the density of conduction electrons and reduces the core-screening of the ionic potential, which in turn modifies the effective screened ion–electron interaction (see the SM). The combined effects lead to the observed minimum and subsequent upturn in the electrical conductivity around this temperature [Fig. 2(a)]. A second, more abrupt increase in Z^* appears near $T \approx 200$ eV, signaling the onset of K-shell ionization. At the ionization onset of both shells, a noticeable inflection appears in the heat capacity C_V [Fig. 4(a)], as a large amount of internal energy is absorbed in liberating tightly bound electrons. At $T \approx 1000$ eV, the ionization is essentially complete and the electrons are weakly degenerate, marking a transition beyond the warm dense matter regime. For comparison, the AA model [53] qualitatively reproduces the shell-ionization signatures in Z^* and C_V at high temperatures, where electrons are nearly fully ionized. However, it fails to capture the correct shape and location of these transitions, particularly in the low- and intermediate-T regimes where bound-state effects are significant. This limitation stems from the hybrid treatment in which the bound states are solved quantum-mechanically, while the free states are described using the Thomas–Fermi approximation, which provides only partial shell resolution.

Conclusion

We introduced an efficient approach that combines the Kubo formalism with the mixed stochastic-deterministic DFT framework,

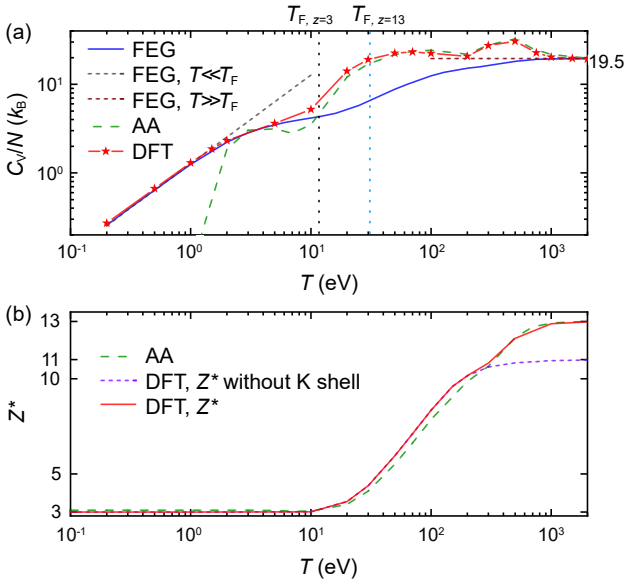

Fig. 4. (a) Electronic isochoric heat capacity and (b) effective ion charge of aluminum at different temperatures. "FEG" denotes results from the free-electron gas model, with $T \ll T_F$ corresponding to the strongly degenerate limit and $T \gg T_F$ to the weakly degenerate limit. "AA" refers to average-atom model results [53]. "DFT" results are obtained from KSDFT at $T \leqslant 10$ eV and from mDFT at higher temperatures.

enabling efficient calculations of electrical conductivity and thermal conductivity. Our results demonstrate that this approach is efficient for calculating the conductivity of high-temperature, dense aluminum up to 1000 eV. The computed electrical and thermal conductivities align well with the results from low-temperature KS-DFT calculations. This work extends the applicability of first-principles conductivity calculations by two orders of magnitude in temperature, establishing a parameter-free benchmark for extreme warm dense matter and hot dense plasma.

This work was supported by the NSFC Excellence Research Group Program (Grant Nos. 12588301 and 12588201) and the National Key R&D Program of China (Grant No. 2025YFB3003603). This work was also supported by the Foundation of National Key Laboratory of Computational Physics, China. The numerical simulations were performed on the High-Performance Computing Platform of CAPT.

References

[1] Hubbard W B 1968 *The Astrophysical Journal* **152** 745
[2] Hsieh W P, Deschamps F, Tsao Y C, Yoshino T, and Lin J F 2024 *Sci. Adv.* **10** eadk1087
[3] Wang Y, Shi J, Liang Z, Huang T, Wang J, Ding C, Pickard C J, Wang H T, Xing D, Ni D, and Sun J 2025 *Nat. Commun.* **16** 5504
[4] Marinak M M, Haan S W, Dittrich T R, Tipton R E, and Zimmerman G B 1998 *Phys. Plasmas* **5** 1125
[5] Hu S X, Collins L A, Boehly T R *et al.* 2014 *Phys. Rev. E* **89** 043105
[6] Kang D, Hou Y, Zeng Q, and Dai J 2020 *Matter Radiat. Extrem.* **5** 055401
[7] Ivanov D S and Zhigilei L V 2003 *Phys. Rev. B* **68** 064114
[8] Weir S T, Mitchell A C, and Nellis W J 1996 *Phys. Rev. Lett.* **76** 1860
[9] Nellis W J, Weir S T, and Mitchell A C 1999 *Phys. Rev. B* **59** 3434
[10] Lorenzen W, Holst B, and Redmer R 2009 *Phys. Rev. Lett.* **102** 115701
[11] Young D A, McMahan A K, and Ross M 1981 *Phys. Rev. B* **24** 5119
[12] Kietzmann A, Holst B, Redmer R, Desjarlais M P, and Mattsson T R 2007 *Phys. Rev. Lett.* **98** 190602
[13] Celliers P M, Loubeyre P, Eggert J H *et al.* 2010 *Phys. Rev. Lett.* **104** 184503
[14] McKelvey A, Kemp G E, Sterne P A *et al.* 2017 *Sci. Rep.* **7** 1
[15] Jiang S, Landen O L, Whitley H D *et al.* 2023 *Commun. Phys.* **6** 98
[16] Allen C H, Oliver M, Gericke D O *et al.* 2025 *Nat. Commun.* **16** 1983
[17] Rhim W K and Ishikawa T 1998 *Rev. Sci. Instrum.* **69** 3628
[18] Brandt R and Neuer G 2007 *Int. J. Thermophys.* **28** 1429
[19] Spitzer L and Härm R 1953 *Phys. Rev.* **89** 977
[20] Spitzer L Jr 2006 *Physics of Fully Ionized Gases* (Dover Publications)
[21] Lee Y T and More R M 1984 *Phys. Fluids* **27** 1273
[22] Ichimaru S and Tanaka S 1985 *Phys. Rev. A* **32** 1790
[23] Hohenberg P and Kohn W 1964 *Phys. Rev.* **136** 864B
[24] Mermin N D 1965 *Phys. Rev.* **137** A1441
[25] Kohn W and Sham L J 1965 *Phys. Rev.* **140** 1133A
[26] Kubo R 1957 *J. Phys. Soc. JPN* **12** 570
[27] Greenwood D A 1958 *Proc. Phys. Soc.* **71** 585
[28] Desjarlais M P, Kress J D, and Collins L A 2002 *Phys. Rev. E* **66** 025401
[29] Recoules V and Crocombette J P 2005 *Phys. Rev. B* **72** 104202
[30] Vlček V, de Koker N, and Steinle-Neumann G 2012 *Phys. Rev. B* **85** 184201
[31] Witte B B L, Sperling P, French M *et al.* 2018 *Phys. Plasmas* **25** 056901
[32] Liu Q, Li J, and Chen M 2021 *Matter Radiat. Extrem.* **6** 026902
[33] Cytter Y, Rabani E, Neuhauser D, and Baer R 2018 *Phys. Rev. B* **97** 115207
[34] Lin F, Morales M A, Delaney K T *et al.* 2009 *Phys. Rev. Lett.* **103** 256401
[35] Faussurier G and Blancard C 2019 *Phys. Rev. E* **100** 033202
[36] Shaffer N R and Starrett C E 2020 *Phys. Rev. E* **101** 053204
[37] Wetta N and Pain J C 2020 *Phys. Rev. E* **102** 053209
[38] Rightley S and Baalrud S D 2021 *Phys. Rev. E* **103** 063206
[39] White A J and Collins L A 2020 *Phys. Rev. Lett.* **125** 055002
[40] Baer R, Neuhauser D, and Rabani E 2013 *Phys. Rev. Lett.* **111** 106402
[41] Cytter Y, Rabani E, Neuhauser D *et al.* 2019 *Phys. Rev. B* **100** 195101
[42] Chen M, Guo G C, and He L 2010 *J. Phys.: Condens. Matter* **22** 445501
[43] Li P, Liu X, Chen M *et al.* 2016 *Comp. Mater. Sci.* **112** 503
[44] Liu Q and Chen M 2022 *Phys. Rev. B* **106** 125132
[45] Nosé S 1984 *J. Chem. Phys.* **81** 511
[46] Hoover W G 1985 *Phys. Rev. A Gen. Phys.* **31** 1695
[47] Chen T, Liu v, Liu Y, Sun L, and Chen M 2024 *Matter Radiat. Extrem.* **9** 015604
[48] Karasiev V V, Sjostrom T, Dufty J, and Trickey S B 2014 *Phys. Rev. Lett.* **112** 076403
[49] Karasiev V V, Dufty J W, and Trickey S B 2018 *Phys. Rev. Lett.* **120** 076401
[50] Liu Q and Chen M 2024 *Phys. Rev. B* **110** 014207
[51] Perdew J P, Burke K, and Ernzerhof M 1996 *Phys. Rev. Lett.* **77** 3865
[52] Monkhorst H J and Pack J D 1976 *Phys. Rev. B* **13** 5188
[53] Callow T J, Kraisler E, and Cangi A 2023 *Phys. Rev. Res.* **5** 013049